Human Pulvinar Functional Organization and Connectivity

Daniel S. Barron,[1,2] **Simon B. Eickhoff,**[3,5] **Mareike Clos,**[4,5] and
Peter T. Fox[1,6,7,8,9,10]*

[1]*Research Imaging Institute, University of Texas Health Science Center at San Antonio, Texas, USA*
[2]*Yale University School of Medicine, New Haven, Connecticut, USA*
[3]*Institute of Neuroscience and Medicine (INM-1), Research Centre Jülich, Jülich, Germany*
[4]*Institute of Clinical Neuroscience and Medical Psychology, Heinrich Heine University, Düsseldorf, Germany*
[5]*Department of Systems Neuroscience, University Medical Center Hamburg-Eppendorf, Hamburg, Germany*
[6]*Department of Radiology, University of Texas Health Science Center at San Antonio, San Antonio, Texas, USA*
[7]*Research Service, South Texas Veterans Health Care System, San Antonio, Texas, USA*
[8]*Department of Neurology, University of Texas Health Science Center, San Antonio, Texas, USA*
[9]*State Key Laboratory for Brain and Cognitive Sciences, University of Hong Kong, Hong Kong*
[10]*Neuroimaging Laboratory, Shenzhen University School of Medicine, Shenzhen, China*

◆ ══════════════════ ◆
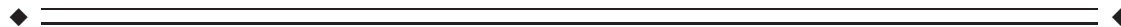
Abstract: The human pulvinar is the largest thalamic area in terms of size and cortical connectivity. Although much is known about regional pulvinar structural anatomy, relatively little is known about pulvinar functional anatomy in humans. Cooccurrence of experimentally induced brain activity is a traditional metric used to establish interregional brain connectivity and forms the foundation of functional neuroimaging connectivity analyses. Because functional neuroimaging studies report task-related coactivations within a standardized space, meta-analysis of many whole-brain studies can define the brain's interregional coactivation across many tasks. Such an analysis can also detect and define variations in functional coactivations within a particular region. Here we use coactivation profiles reported in ∼ 7,700 functional neuroimaging studies to parcellate and define the pulvinar's functional anatomy. Parcellation of the pulvinar's coactivation profile identified five clusters per pulvinar of distinct functional coactivation. These clusters showed a high degree of symmetry across hemispheres and correspondence with the human pulvinar's cytoarchitecture. We investigated the functional coactivation profiles of each resultant pulvinar cluster with meta-analytic methods. By referencing existent neuroi-

maging and lesion-deficit literature, these profiles make a case for regional pulvinar specialization within the larger human attention-controlling network. Reference to this literature also informs specific hypotheses that can be tested in subsequent studies in healthy and clinical populations. *Hum Brain Mapp 00:000–000, 2015.*   © 2015 **Wiley Periodicals, Inc.**

Key words: pulvinar; functional anatomy; fMRI; cognitive neuroscience; attention

INTRODUCTION

The human pulvinar is the largest thalamic complex and one of the most widely connected with the cerebral cortex. Pulvinar functional anatomy varies greatly across species, reflecting the pulvinar's dramatic evolutionary expansion [Chalfin et al., 2007]. While the pulvinar's visual connections are conserved across higher mammals, it has been suggested that additional neural migrations in humans permit high-level, associative processes unique to our species [Letinic and Rakic, 2001].

The pulvinar's evolutionary accumulation of higher-level function sets the human pulvinar at a phylogenic distance from other species and complicates across-species comparison. This complexity has perhaps fueled the development of largely separate pulvinar literatures that one reviewer describes as "sufficiently taxing, that only aficionados would ever commit much of it to working memory" [Shipp, 2003]. An older, non-human primate (mainly macaques) visual literature describes the pulvinar as a retinotopically organized, visual information-processing center [Shipp, 2003, 2004]. Recently developed methods have led to a cortical-pulvinar-cortical literature that expands pulvinar influence to include attentional [Robinson and Petersen, 1992], executive [Posner and Dehaene, 1994], sensorimotor [Romanski et al., 1997; Wilke et al., 2010], emotional [Ward et al., 2007], and mnemonic [Rotshtein et al., 2011] networks. Recent work in non-human primates [Shipp, 2003] and in humans [Arend et al., 2008] has also shown spatially dissociable gradients of pulvinar connectivity with the cortex. The pulvinar has thereby been implicated in pancortical communication [Saalmann and Kastner, 2011; Shipp, 2003] and alpha rhythm modulation [Saalmann et al., 2012].

Pulvinar connectivity with numerous cortical areas has been confirmed in humans both functionally, using resting-state functional magnetic resonance imaging (fMRI) [Stein et al., 2000] and structurally, using MRI diffusion tensor imaging tractography [Leh et al., 2008]. Disease-related alterations in the pulvinar have been observed in schizophrenia [Byne et al., 2001; Mitelman et al., 2006], epilepsy [Barron et al., 2014; Rosenberg et al., 2009], attention deficit disorder [Ivanov et al., 2010], and spatial neglect [Arend et al., 2008]. This suggests that pulvinar subregions could serve as potential disease markers and therapeutic targets. A comprehensive investigation of the pulvinar's functional subdivisions in healthy humans would thus assist our understanding of pulvinar involvement in human disease, provide a standard for across-group and across-subject integration, and inform future studies.

Regional parcellations of the brain are most definitive when performed independently by converging techniques, ideally by combining cytoarchitecture, connectivity, and function [Felleman and Van Essen, 1991]. While both the non-human primate [Olszewski, 1952] and human [Morel et al., 1997] pulvinar have been described in terms of cytoarchitecture, our knowledge of regional pulvinar anatomical connectivity has been limited to non-human primates, as the invasiveness of anatomical tracer techniques precludes their use in humans [Koski and Paus, 2000]. Cooccurrence of experimentally induced brain activity across regions is a traditional metric used to establish interregional brain connectivity [Paus et al., 1997] and forms the foundation of functional neuroimaging connectivity analyses. Meta-analysis of many whole-brain functional neuroimaging studies can define the brain's interregional coactivation across many tasks and detect variations in functional coactivation within a particular region [Koski and Paus, 2000]. Extending this strategy, we parcellate and describe the human pulvinar's regional functional anatomy by meta-analysis of ~7,700 published functional neuroimaging experiments that represent ~30,000 human subjects. We also validate our results by reference to cytoarchitecture reported by Morel et al. [1997].

METHODS

Two related meta-analytic methods were employed to assess the human pulvinar's functional coactivation: meta-analytic connectivity modeling (MACM) and MACM coactivation-based parcellation (MACM-CBP). The concept underlying these meta-analytic methods is that *x-y-z* foci reported in individual functional neuroimaging experiments represent spatially distinct, functionally connected neurophysiologic events that are active under a given experimental condition [Paus et al., 1997]. By combining across many experiments, the potential errors and bias of each experiment are averaged out and the functional coactivation of a given region can be assessed more accurately. As applied here, functional coactivation is indicated when a group of regions cooccur at rates significantly greater than chance [Bzdok et al., 2013; Cieslik et al., 2013; Koski and Paus, 2000; Toro et al., 2008].

MACM coactivation profiles have been validated by reference to resting-state [Cieslik et al., 2013; Rottschy et al.,
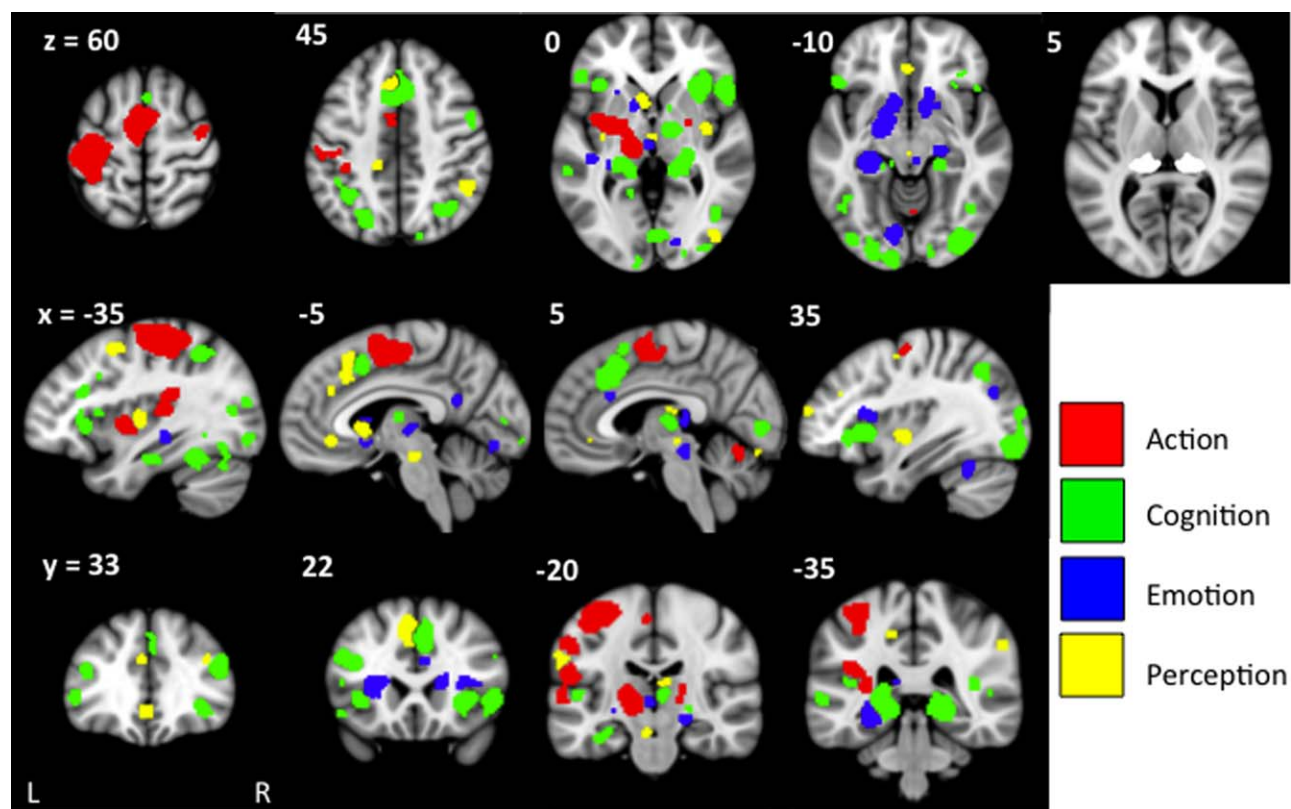
Figure 1.

Pulvinar functional connectivity profiles produced by meta-analytic connectivity modeling (MACM) filtered by BrainMap behavioral domain. Regions indicate statistically significant ($P < 0.05$) differences in coactivation likelihood specific to each behavioral domain. Slice position (given by x, y, or z location) corresponds to the Montreal Neuroimaging Institute's (MNI-152) template space. NB: z=5 depicts the pulvinar region of interest, as defined by Krauth et al. [2010].

2013; Smith et al., 2009], diffusion tractography [Cauda et al., 2011; Eickhoff et al., 2010; Robinson et al., 2012], electrophysiology [Narayana et al., 2012], and non-human primate tracer studies [Robinson et al., 2010]. We also employed MACM-CBP to map the pulvinar in terms of its functional subdivisions. Conceptually, MACM-CBP first creates a functional coactivation map for each voxel in the pulvinar seed volume and then sorts voxels into clusters based on the similarity of these coactivation maps. MACM-CBP therefore yields a parcellation map, with clusters of pulvinar voxels representing similar functional coactivation. MACM-CBP parcellation maps have been validated by reference to resting state studies [Bzdok et al., 2013; Clos et al., 2013]. Below, we describe the selection of our pulvinar volume of interest (VOI) as well as the implementation of MACM and MACM-CBP.

VOI Definition: Morel (1997)

Pulvinar seed regions were defined by Krauth et al.'s [2010] digital 3-D version of the Morel (1997) human tha-lamic atlas in MNI152 space [Krauth et al., 2010; Morel et al., 1997], as shown in Figure 1. The Morel atlas subdi-vides the thalamus based on cytoarchitecture. Because we wanted to test whether MACM-CBP would subdivide the pulvinar along its cytoarchitectural boundaries, we com-bined anterior, medial, lateral, and inferior pulvinar labels to form two pulvinar seed volumes (one per hemisphere).

Bilateral Pulvinar MACM Functional Coactivation

Functional neuroimaging experiments that activate the pulvinar were identified by comparing the x-y-z foci within the Morel pulvinar seed regions with eligible functional mapping experiments contained within the BrainMap data-base (www.brainmap.org). BrainMap is a manually curated, community accessible environment that stores activation foci for published functional neuroimaging studies, as well as experimental and behavioral meta-data associated with each entry (e.g. number of subjects, neuroimaging modality, behavioral domain, paradigm of the contrast) [Fox et al., 2005; Laird et al., 2011]. At the time of analysis, BrainMap

contained ~2,300 published functional neuroimaging papers reporting ~89,000 foci from ~11,000 experiments, representing ~45,000 subjects. The present MACM included only fMRI and positron emission tomography (PET) experiments from "normal mapping" studies (no interventions, no group comparisons) in healthy subjects that reported coordinates in stereotaxic space. Based on this criteria, 1,991 papers reporting 66,657 brain activation locations from 7,772 experiments, representing 29,597 subjects were available for the present analysis.

Relevant functional neuroimaging that reported activation in the bilateral pulvinar VOI were identified using Sleuth 2.1 (brainmap.org/sleuth). Contrasts were limited to fMRI and PET experiments reporting activations (not deactivations) within the bilateral pulvinar; no search restriction was made regarding the nature of task employed in each study. Whole-brain coordinates of activations from identified contrasts were downloaded; this included 3,556 foci from 191 normal mapping experiments in 162 papers representing 2,295 healthy subjects. To insure that neither right nor left pulvinar biased the search results, pulvinar VOIs were searched separately but not analyzed at this stage (left pulvinar retrieved 2,148 foci from 117 experiments representing 1,524 subjects; right pulvinar retrieved 1,229 foci from 87 experiments representing 1,096 subjects). Contrasts were retrieved from all BrainMap behavioral domains. For the bilateral pulvinar VOI, 44% of the experiments retrieved were coded as cognition (90 experiments), 17% as action (35), 18% as emotion (37), 15% as perception (30), and 4% as interoception (9).

Activation likelihood estimation (ALE) meta-analysis was performed on the set of coordinate/location identified to identify significant areas of coactivation with the bilateral pulvinar. ALE models each reported coordinate as a Gaussian distribution reflecting empirical estimates of the uncertainty of different spatial normalization techniques. Rather than utilizing a user-defined full-width half maximum (FWHM) as in the original ALE approach [Turkeltaub et al., 2002], an algorithm was used to model the spatial uncertainty of each focus based on the estimation of the intersubject and interlaboratory variability typically observed in neuroimaging experiments [Eickhoff et al., 2009]. This algorithm includes individual FWHM values for each experiment that are weighted by the sample size of the original study, thereby allowing experiments with largest numbers of subjects to be weighted more strongly than those with fewer subjects. ALE was performed using GingerALE 2.1 [Eickhoff et al., 2009]. Modeled activation (MA) maps were computed by pooling all activation foci's probability distributions reported in a given experiment [Turkeltaub et al., 2012]. MA maps contain per-voxel probability of activation being located at that voxel (throughout the brain) in a given experiment. ALE scores were then calculated on a voxel-by-voxel basis by taking the union of these individual MA maps. Spatial inference on meta-analysis aims at identifying those voxels where the convergence across all MA maps is higher than expected if the

results were independently distributed. The ALE scores were then tested for significance in a random-effects analysis against a null distribution reflecting a random spatial association between experiments [Eickhoff et al., 2012]. Resultant ALE maps were thresholded to include only foci with a cluster-level threshold of $P_{corrected} < 0.001$ (corrected for family-wise error rate as described in Eickhoff et al. [2012] and converted to z-scores for visualization). This first ALE analysis served as a "global" meta-analytic connectivity model, encompassing all behavioral domains.

Bilateral Pulvinar Behavioral Domain-Specific MACM Functional Connectivity

Because the BrainMap meta-data taxonomy [Fox et al., 2005] classifies each functional neuroimaging experiment by the behavioral domain activated in its respective task, each MACM coactivation profile can be built specific to each behavioral domain by restricting BrainMap queries to experiments with a particular domain. Accordingly, the above BrainMap search results were restricted to each behavioral domain category (e.g. action, cognition, emotion, and perception) and the whole-brain ALE meta-analyses were repeated separately for foci reported within each behavioral domain. Because of the relatively small number of experiments retrieved for interoception (nine experiments), ALE was not performed for this behavioral domain.

Contrast analyses were then computed for each behavioral domain to determine where in the brain each behavioral domain is represented more than other domains. Contrast analysis computes the voxel-wise difference between ALE scores for the two sets of coactivation foci [Eickhoff et al., 2011]. For example, to determine where action is represented in the brain versus all other behavioral domains, all experiments contributing to these two groups (group 1: action; group 2: cognition, memory, perception) were pooled and randomly dividing into two groups of the same size. That is, given 56 BrainMap experiments were coded within the action domain and 205 experiments were coded in all other domains, the resultant pool (261 total) would be randomly divided into groups of 56 and 205. ALE scores for these two randomly assembled groups were then calculated and the difference between ALE scores was recorded for each voxel in the brain. Repeating this process 10,000 times yielded a null distribution for the differences in ALE scores between the behavioral domains MACM analyses, i.e., action and all others (cf. Fig. 1). The observed difference was then tested under this null distribution by thresholding for a posterior probability of $P > 0.99$ for true differences and additionally by masking with the significant main effect for $P_{corrected} < 0.01$ in the primary analysis for the seed region showing the larger ALE score.

MACM-CBP of Unilateral Pulvinar

MACM-CBP of right and left pulvinar VOIs was performed using the BrainMap database. MACM-CBP has
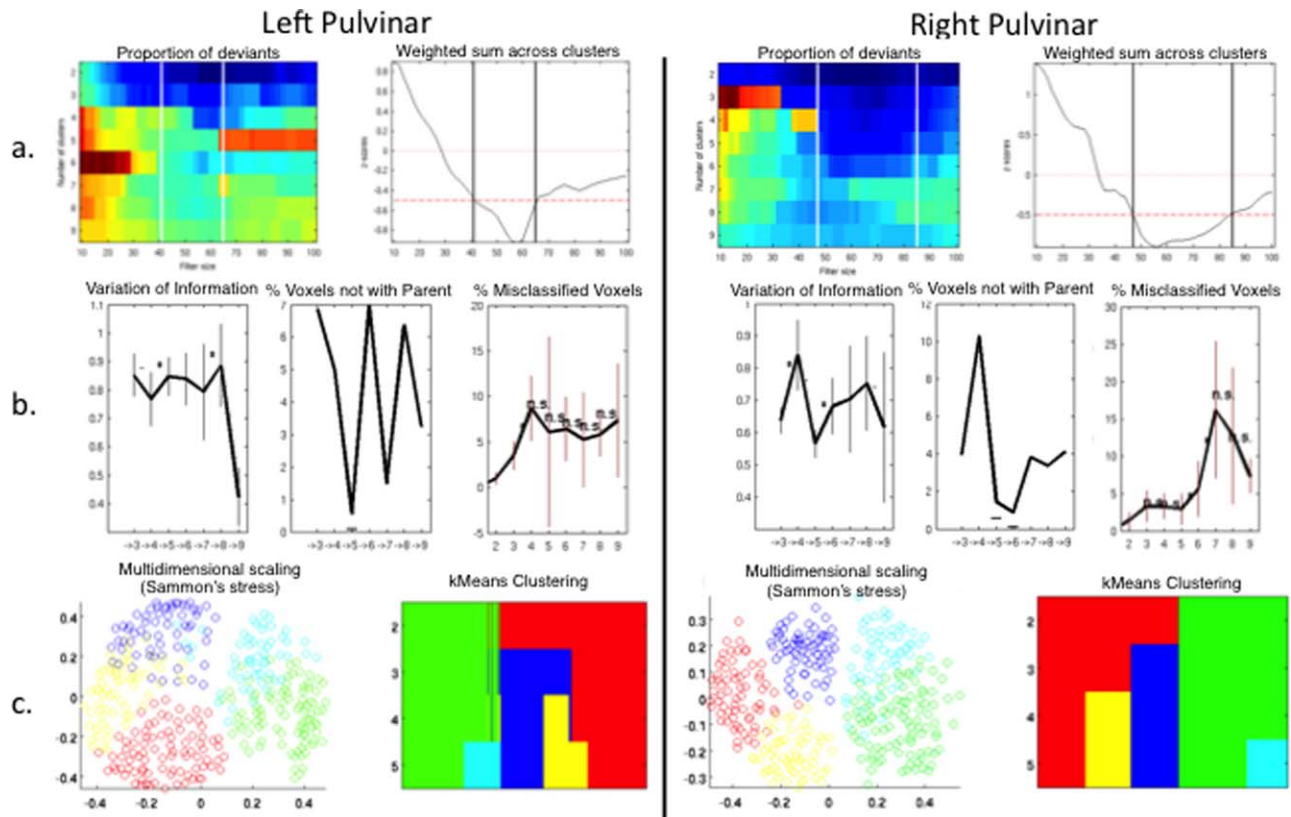
Figure 2.

Spatial Filter and Cluster Criteria. (**A**) Vertical lines specify the most stable range of filter sizes based on the proportion of deviants computed across filter size (left; hot=high, cold=low) and on the maximum z-score of median-filtered deviants (right). (**B**) Criteria supporting a five cluster solution include variation of information (left), percentage of voxels not with parent (cen-ter), and percentage of misclassified voxels (right). (**C**) Visualiza-tion of five cluster solution by multidimensional scaling (left, proximity indicates similar voxel coactivation patterns) and pat-tern of cluster assignment and splitting of clusters across levels of K (right).

been thoroughly described and validated elsewhere [Bzdok et al., 2013; Clos et al., 2013]; however, for the con-venience of the reader, we outline this process below. Because MACM-CBP is a voxel-wise parcellation tech-nique, a reliable per-voxel modeled activation (MA) map must be created for each experiment that coactivates with this voxel. However, a general problem of this meta-analytic mapping is that some voxels are not activated by a sufficiently high number of experiments to allow a robust analysis [Bzdok et al., 2013]. To enable a reliable delineation of task-based functional connectivity, we used a spatial filter to pool across the neighborhood of each VOI voxel and identify BrainMap experiments that reported activation closest to each VOI voxel (Fig. 2A). This spatial filter was achieved by calculating and then sorting the Euclidean distance between a given VOI voxel and all activations within BrainMap. The extent of the spa-tial filter was systematically expanded about each VOI voxel to create a coactivation map for the closest 10 up to

the closest 100 associated BrainMap experiments in steps of two (i.e., closest 10, 12, 14, . . .,100 experiments making 46 different filter sizes).

The retrieved activations were then used to compute the brain-wide coactivation profile for each VOI voxel at each of the 46 filter sizes. This profile was computed with the ALE algorithm to produce a MA map for each VOI voxel, each MA map representing a summation across individual Brain-Map experiments. The ALE scores of all voxels within the gray matter [based on 10% probability according to the ICBM (International Consortium on Brain Mapping) tissue probability maps] were then recorded before moving to the next VOI voxel. Because no inference was sought at this point of the analysis, the MA map was not thresholded. Rather, the aim was to record for each seed voxel the "full" individual probability of coactivation with all other brain voxels and to use this profile in subsequent parcellation.

The unthresholded brain-wide coactivation profiles for all VOI voxels were combined into an N_RxN_B connectivity

matrix, where N_R is the number of VOI voxels (2,380 for R pulvinar, 2,385 for L pulvinar at $1 \times 1 \times 1mm^3$) and N_B is the number of whole-brain voxels (~260,000) voxels within the gray matter at $2 \times 2 \times 2mm^3$ resolution. VOI voxels with similar brain-wide coactivation profiles were identified by K-means clustering as implemented in MatLab (2012a, Mathworks, Natick MA) with K=2, 3, ...,9 using one minus the correlation between the coactivation patterns of the individual seed voxels as the distance measure (correlation distance) [Clos et al., 2013]. This parcellation was performed independently for each of the 46 spatial filters, yielding 8 (K number of clusters) × 46 (filter size) independent cluster solutions (Fig. 2A) [Clos et al., 2013]. K-means is an iterative, nonhierarchical clustering method that parcellates a seed region into K nonoverlapping clusters by minimizing the within-cluster variance of each seed voxel from the (randomly initialized) centroids. The reason for using K-means rather than hierarchical clustering is that, by design, hierarchical clustering is sensitive to local, individual voxel features and does not allow individual voxels to change cluster assignment once specified. This may lead to optimal local groupings, but nonoptimal global solutions. K-means was applied to overcome this issue, however, to ensure that hierarchically consistent clusters were reported, a pseudohierarchical K-means clustering was used wherein hierarchically inconsistent voxels (voxels that were assigned to different clusters depending on cluster solution) were removed from the final cluster solution [Clos et al., 2013]. For each of the 8 × 46 parcellations, the best solution from 100 replications was recorded. In sum, the VOI voxels were thus merged as a function of correspondence of their coactivation profiles, thus parcellating the L and R pulvinar into clusters of similar functional coactivation networks.

For each of the 46 spatial filter sizes, the K-means procedure yielded eight different solutions parcellating each pulvinar into 2, 3,.,9 subdivisions (Fig. 2A). The properties of each filter size and cluster solution were recorded and, based on these properties, the optimal spatial filter range and cluster solution were chosen.

The optimal spatial filter was selected as a range of filter sizes. The upper and lower limits of this range was determined as filter sizes that showed a significant increase (z-normalized score) of inconsistently classified voxels greater and less than that range (Fig. 2B, also Supporting Information Figures S1 and S2). In all subsequent steps, the analysis was restricted to K parcellations based on the nearest 42–66 experiments for the L pulvinar and 48–84 experiments for the R pulvinar.

The optimal K cluster solution was based on the topological and information-theoretic properties of each solution (Fig. 2B). The first topological criterion was the percentage of voxels not hierarchically related to the dominant parent cluster compared to the K-1 solution (middle panel, Fig. 2B). That is, a given K cluster parcellation qualified as a good solution if the percentage of voxels not with the parent (lost because they were not hierarchically

consistent) was below the median across all steps and the following clustering-step featured a local maximum in the percentage of lost voxels. The second topological criterion considered the percentage of misclassified voxels as an indirect reflection of the amount of noise and potentially local effects in the clustering (right panel, Fig. 2B). In particular, the criterion addressed the across-filter stability, that is, the average percentage of voxels for each filter-size that were assigned to a different cluster compared to the most frequent (mode) assignment of these voxels across all filter sizes. Good K solutions were those where the percentage of misclassified voxels did not significantly increase compared to the K-1 solution and/or where subsequent K+1 solution led to a significant higher percentage of misclassified voxels. The information-theoretic criterion considered the similarity of cluster assignments between the current and neighboring solutions (solution K compared to K-1 and K+1) based on variation of information (VI) metrics (left panel, Fig. 2B). VI measurements is an established clustering criterion for determining the optimal K-means parcellation of a given brain region. [Kahnt et al., 2012; Kelly et al., 2010] For each filter size, the VI metric was computed between K and K+1 solutions. The VI between two cluster solutions, C and C' was computed as

$$VI(C, C')_k = H(C)_k + H'(C')_k - 2I(C, C')_k$$

Where H represents the amount of information (entropy) present in the cluster solutions C and C' and I is the mutual information shared by the two cluster solutions. A good solutions K showed a significant increase in VI from K to K+1 (primary criterion), and/or a significant decrease in VI from K-1 to K (secondary criterion).

Visualization of the Best Cluster Solution

For both R and L pulvinar VOIs (performed independently), a five cluster solution was identified as the most stable parcellation by the above criteria. Within these parcellations, subsequent analyses were restricted to hierarchically consistent voxels (explained above), which reduced the resultant overall VOI voxel number (R pulvinar decreased from 2,380 to 2,013 voxels; L pulvinar decreased from 2,385 to 2,082 voxels). To visualize the dissimilarity in whole-brain coactivation profiles for each cluster, multidimensional scaling (MDS) was used (Fig. 2C). MDS allows signals in N-dimensional "functional space" to be represented in 2-D. To this end, first the pairwise correlation (minus one) between the coactivation profiles of individual VOI voxels was computed across the selected filter size range (described above), thus forming a distance matrix N_R x N_R. MDS was performed on the eigenimage of this distance matrix using Sammon's nonlinear mapping as the goodness-of-fit criterion. For each hemisphere, the five cluster pulvinar parcellation was mapped back to the brain (MNI152 space) for anatomical visualization (Fig. 3). To validate this parcellation, correspondence with the
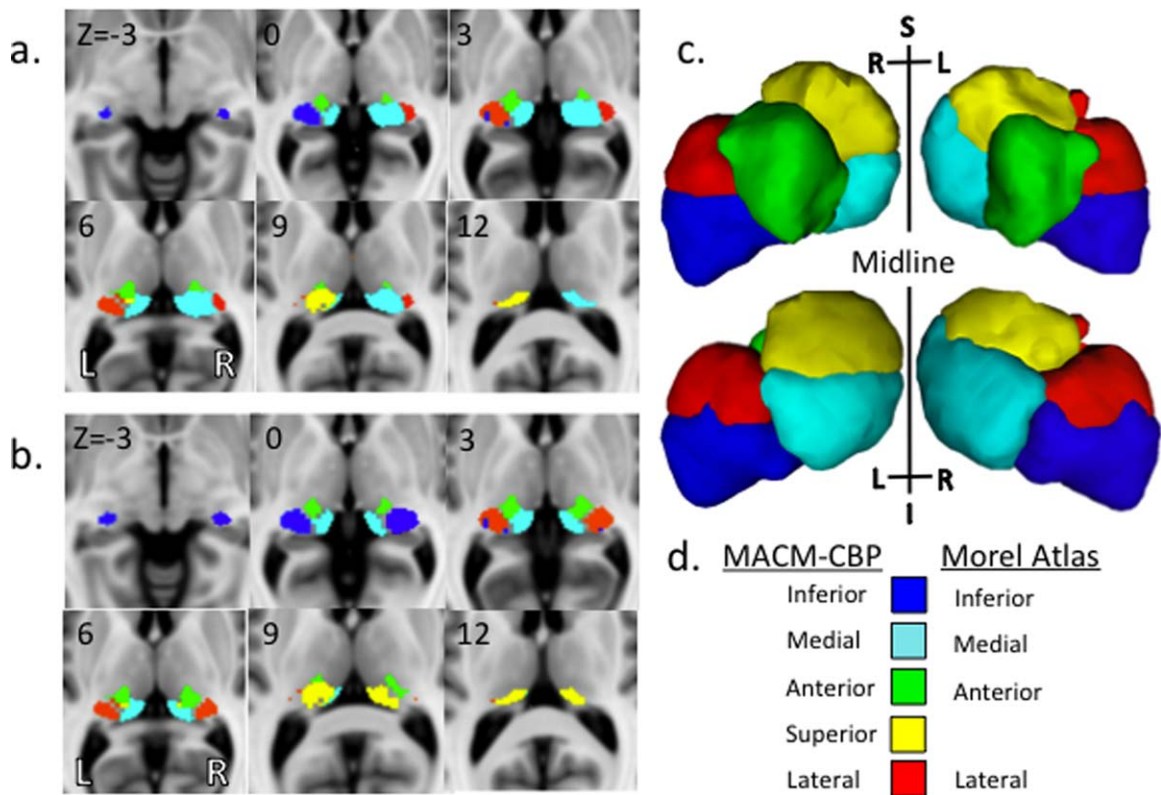
Figure 3.

Comparison of left and right pulvinar parcellations. (**A**) Correspondence between the pulvinar coactivation-based parcellation (left hemisphere) and the Morel thalamic atlas (right hemisphere) (**B**) Symmetry between the independent left and right hemisphere pulvinar coactivation-based parcellations. (**C**) Three-dimensional surface rendering of the left and right MACM-CBP clusters as viewed from the anterior (above) and the posterior aspect (below) oriented about the midline. (**D**) Color key for MACM-CBP cluster labels in this and subsequent figures. (NB: Morel Atlas is only shown in the right hemisphere of Figure 3A) Slice position (given by x, y, or z location) corresponds to the Montreal Neuroimaging Institute's (MNI-152) template space.

Morel cytoarchitectonic atlas as determined by means of an percent overlap calculated as the number of overlapping Morel and MACM-CBP voxels divided by the number of Morel voxels (cf. Table I).

Analysis of Cluster-Specific Task-Dependent Connectivity

To characterize the coactivation pattern for each of the five MACM-CBP clusters per pulvinar, a follow-up MACM analysis was performed using methods described above (Figs 4–6)[Eickhoff et al., 2011]. A conjunction analysis was performed for each hemisphere, to determine which brain regions were coactivated across all five clusters. In addition, contrast analysis was performed to reveal which brain regions were significantly more coactivated with a given cluster than with other clusters. The latter contrast analysis produced a cluster-specific co-activation pattern or task-dependent coactivation profile. This coactivation pattern was described in tabular form in terms of coactivation cluster volume, maximum value and location, and coactivation center-of-gravity (cf. Supporting Information Table SI).

Automated Cluster-Specific Behavioral Interpretation

The BrainMap database curates experimental and behavioral meta-data associated with each entry [Fox et al., 2005]. Meta-data can be exploited to provide behavioral categorizations (including statistical differences from the whole-brain distributions) for brain areas and systems [Lancaster et al., 2012]. Prior MACM-CBP studies have used this tool with success [Bzdok et al., 2013; Clos et al., 2013]. In the present instance, this approach was unsuccessful (see Results, Discussion).

TABLE I. Overlap of the pulvinar MACM-CBP clusters and the Morel cytoarchitectonic thalamic atlas in terms of percentage (above) and voxel quantity (below)

Percent overlap of Morel with MACM-CBP

	Left hemisphere						Right hemisphere				
	I	M	A	S	L		I	M	A	S	L
PuA	-	-	98%	-	-	PuA	-	-	93%	-	-
PuI	100%	-	-	-	-	PuI	100%	-	-	-	-
PuL	47%	-	-	-	39%	PuL	42%	-	-	-	46%
PuM	18%	28%	10%	21%	11%	PuM	19%	20%	14%	20%	9%

Voxel overlap of Morel with MACM-CBP

	Left Hemisphere							Right Hemisphere					
	I	M	A	S	L			I	M	A	S	L	
PuA	-	-	164	-	-	164	PuA	-	-	158	-	-	158
PuI	59	-	-	-	-	59	PuI	62	-	-	-	-	62
PuL	181	-	-	-	150	331	PuL	167	-	1	-	184	352
PuM	326	506	176	383	193	1584	PuM	344	373	261	364	171	1513
	566	506	340	383	343	2138		573	373	420	364	355	2085

Percent overlap was calculated as the number of overlapping Morel and MACM-CBP voxels (for each corresponding row/column pair) divided by the number of Morel voxels. Pulvinar nuclei abbreviations applied from Morel et al. [1997]: anterior pulvinar, PuA; medial pulvinar, PuM; inferior pulvinar, PuI; lateral pulvinar, PuL. MACM-CBP cluster abbreviations: anterior cluster, A; inferior cluster, I; medial cluster, M; lateral cluster, L; superior cluster, S.

RESULTS

Unfiltered MACM

An unfiltered (behaviorally) MACM was performed to assess the bilateral pulvinar's overall coactivation profile. Results showed wide-spread task-based coactivation representing the main effect across all behavioral domains and pulvinar regions. This unfiltered MACM is not presented in a figure.

Behaviorally Filtered MACM Contrasts

An additional MACM filtered by behavioral domain was performed to assess where the bilateral pulvinar was significantly more likely to coactivate one behavioral domain than another. The contrast analysis of these MACMs showed spatially discrete regions of coactivity for each behavioral domain (cf. Fig. 1).

Action-specific regions of coactivation with the pulvinar were observed in somatosensory regions, basal ganglia, and cerebellum. Cognition-specific regions of coactivation were seen in the middle and medial frontal gyrus, anterior cingulate, insula, superior and inferior temporal lobe, occipital (visual) areas, and parahippocampus. Emotion-specific regions of coactivation were seen in the amygdala, lentiform nuclei, and lingual gyrus. Perception-specific regions were minimally represented but included coactivations in the medial and middle frontal gyrus, anterior cingulate, and caudate head.

MACM-CBP of Left and Right Pulvinar

Independently performed MACM-CBP analyses of the R and L pulvinar both indicated a five cluster solutions as the best parcellation of the seed volume based on the whole-brain coactivation profiles (cf. Fig. 2). For both analyses, all clustering parameters were well behaved and within the ranges of previously reported MACM-CBP studies [Bzdok et al., 2013, 2013; Cieslik et al., 2013; Clos et al., 2013].

The visualization in 2-D, the hierarchical splitting of the five clusters and their anatomical location in the brain are displayed in Figure 2C. At K=2, both pulvinars were composed of an anteromedial $_{K=2}$ cluster (green in Fig. 2C) and a posterolateral$_{K=2}$ cluster (red). At the next level K=3, in L pulvinar's posterolateral$_{K=2}$ cluster split into a lateral $_{K=3}$ (red) and posterior $_{K=3}$ (blue) cluster while the R pulvinar's posterolateral$_{K=2}$ cluster split into a superolateral $_{K=3}$ (red) and inferior $_{K=3}$ (blue) cluster. At K=4, the L pulvinar's posterior$_{K=3}$ cluster (blue) split to produce an inferior $_{K=4}$ (blue) and superior $_{K=4}$ (yellow) cluster; whereas the R pulvinar's superolateral $_{K=3}$ (red) cluster split to produce a superior $_{K=4}$ (yellow) and lateral $_{K=4}$ (red) cluster. At K=5, in both pulvinars the anteromedial$_{K=1}$ cluster split into anterior$_{K=5}$ (green) and medial $_{K=5}$ (light blue) clusters.

An overlap analysis was used to compare the MACM-CBP anterior, medial, lateral, inferior, and superior pulvinar clusters to the Morel anterior (PuA), inferior (PuI),
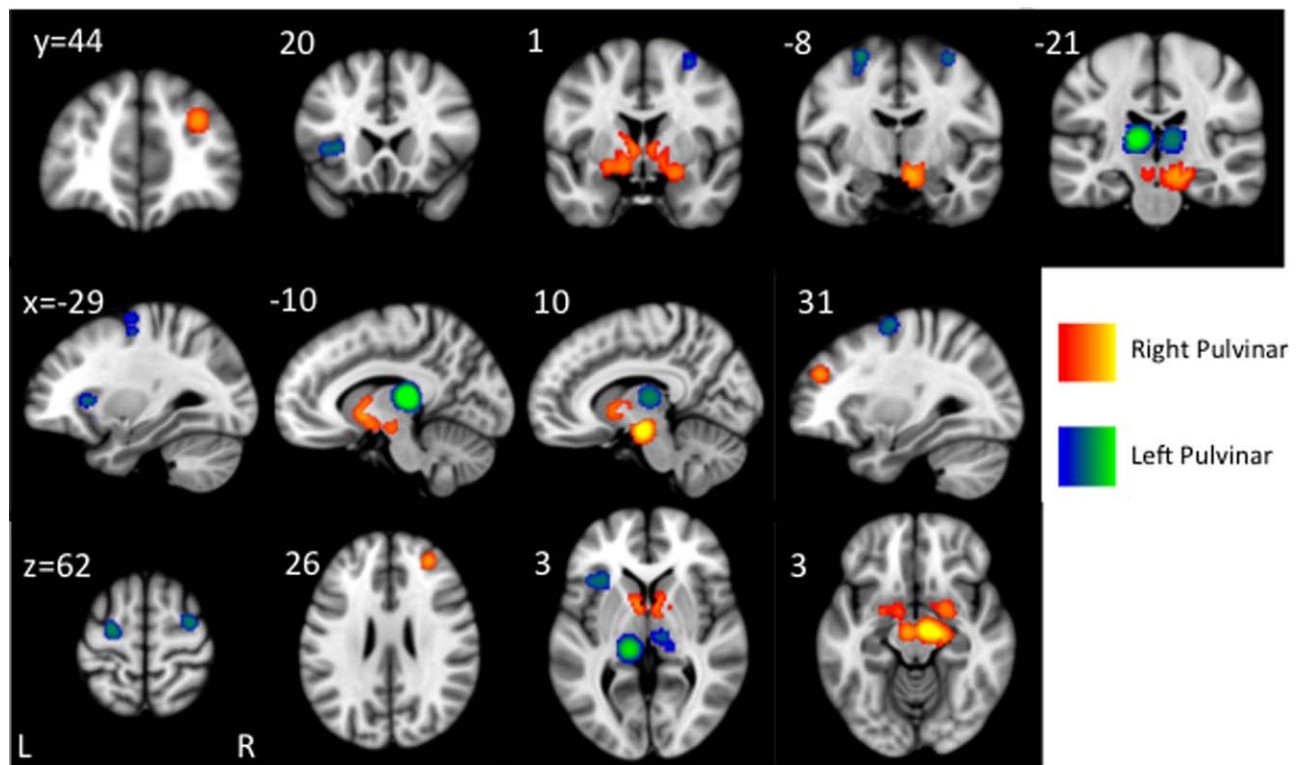
Figure 4.

Conjunction analysis for separate L and R pulvinar MACM-CBP analyses. In the L pulvinar, significant coactivation across all five clusters was observed in bilateral medial thalamic, bilateral middle frontal gyrus, and ipsilateral insular regions (blue-green spectrum). In the R pulvinar, significant coactivation across all five clusters was observed in ipsilateral superior frontal gyrus and bilateral basal ganglia (red-yellow spectrum). Slice position (given by x, y, or z location) corresponds to the Montreal Neuroimaging Institute's (MNI-152) template space.

lateral (PuL), and medial (PuM) pulvinar labels. Similar results were seen across L and R MACM-CBP solutions (cf. Fig. 3A, Table I). The PuA was almost completely contained within the anterior MACM-CBP cluster. The PuI was almost completely contained within the inferior MACM-CBP cluster. The PuL was split, nearly equally, between the inferior and lateral MACM-CBP clusters. The PuM, the largest of the Morel labels, was distributed among all five MACM-CBP clusters nearly equally. Therefore, MACM-CBP clusters showed both strong similarities with and noteworthy divergences from the Morel atlas, discussed below.

Behavioral interpretation of individual pulvinar clusters was unsuccessful; pulvinar clusters were not significantly different (behaviorally) from the whole-brain distribution (cf. Discussion).

Analysis of Cluster-Specific Task-Dependent Connectivity

Additional MACM analyses were performed to further characterize each pulvinar cluster. For each hemisphere, the coactivation patterns common to all five clusters were investigated via conjunction analysis (cf. Fig. 4). In the L pulvinar, all five clusters showed connectivity with the bilateral medial thalamus, bilateral middle frontal gyrus, and L anterior insula. In the R pulvinar, all five clusters showed coactivation with the R superior frontal gyrus and bilateral basal ganglia.

Each pulvinar cluster was characterized in terms of its specific coactivation pattern, e.g. regions to which it alone projected (cf. Figs. 5, 6, and Supporting Information Table SI). This specific MACM analysis extended the lateralized effects observed in the conjunction analysis (reported above) with specific coactivations for each cluster. While all coactivated regions may be referenced in Supporting Information, only major coactivated regions are listed here in the text. In the L pulvinar, the anterior cluster coactivated with the L precentral and post central gyrus, R cerebellum, L putamen, and bilateral medial frontal gyrus; the medial cluster coactivated with the bilateral anterior cingulate, superior colliculus, pretectum, and medial thalamus (pulvinar); the lateral cluster coactivated with the L posterior superior parahippocampus; the inferior cluster
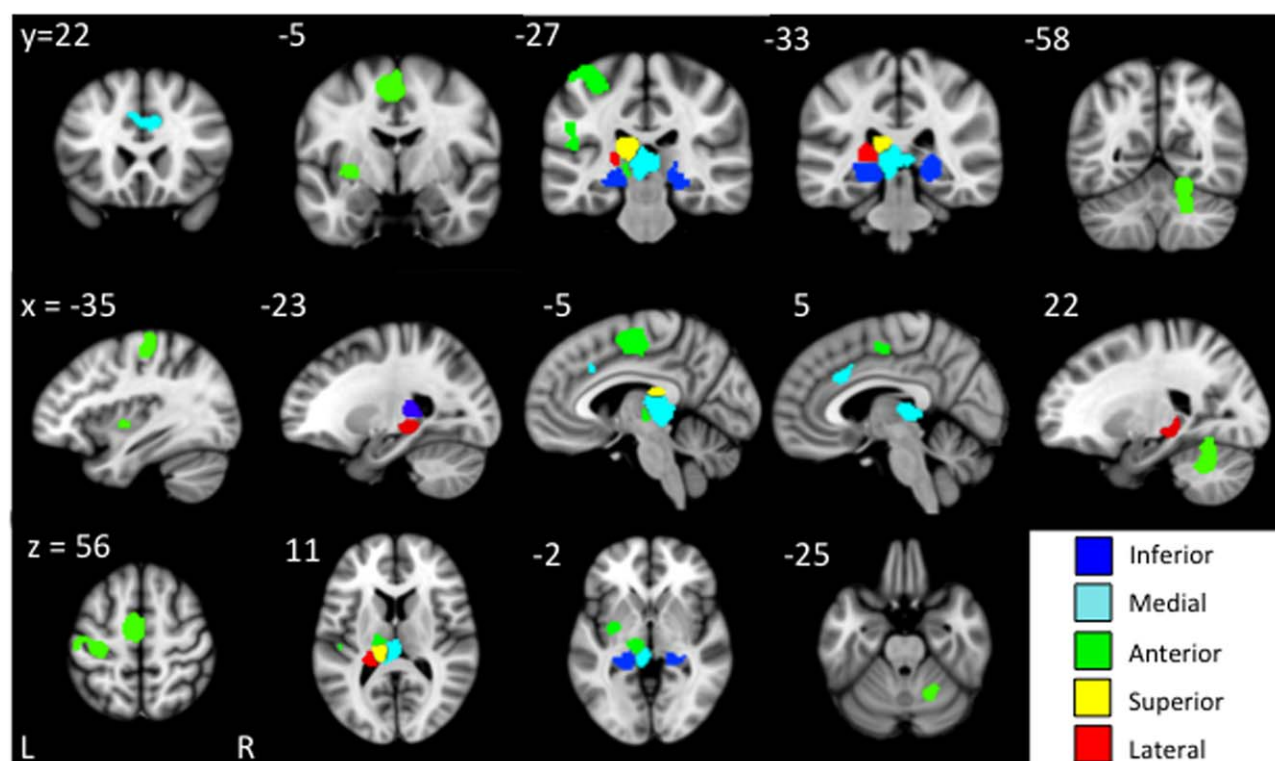
Figure 5.

Left pulvinar cluster specific task-based coactivation. For further description, cf. Results and Discussion. Slice position (given by x, y, or z location) corresponds to the Montreal Neuroimaging Institute's (MNI-152) template space.

coactivated with the bilateral posterior inferior parahippocampus and lateral pulvinar; the superior cluster coactivated with L pulvinar.

In the R pulvinar, the anterior cluster coactivated with the L cerebellum, L Broca's region, and R superior temporal gyrus; the medial cluster coactivated with R middle frontal gyrus, R inferior substantia nigra, and R red nucleus; the lateral cluster coactivated with the L lateral amygdala, hippocampus, and lentiform nucleus; the inferior cluster coactivated with the bilateral amygdala; the superior cluster coactivated with the bilateral superior red nucleus and superior colliculus.

DISCUSSION

The human pulvinar's functional organization and coactivation distribution was defined by meta-analysis of ∼7,700 published functional neuroimaging experiments representing ∼30,000 subjects. Parcellation of the pulvinar's coactivation profile identified five clusters per pulvinar, each cluster representing a region with distinct functional coactivation. Clusters defined by this parcellation showed a high degree of interhemispheric symmetry

and a high correspondence to cytoarchitectural divisions reported in the Morel atlas. The functional coactivation of each resultant pulvinar cluster was modeled with meta-analytic methods. In each hemisphere, coactivation distributions common to all five clusters and specific to each cluster were defined. These distributions are supported by reference to previous neuroimaging and lesion-deficit studies of the pulvinar.

Pulvinar Cluster Correspondence with the Morel Cytoarchitecture

Substantial overlap of the MACM-CBP clusters with the cytoarchitecture reported in the Morel atlas provides a foundation for MACM-CBP's biological validity [Felleman and Van Essen, 1991]. MACM-CBP divisions aligned best with the smaller Morel cytoarchitectural regions, e.g. the PuA and PuI (cf. Table I). Because each MACM-CBP cluster represents a region of distinct task-based connectivity, divergences from the cytoarchitecture are informative. The larger the cytoarchitectural region, the more it was broken up by MACM-CBP; e.g. the PuL (∼340 voxels) was broken up into two MACM-CBP clusters; the PuM, the largest of
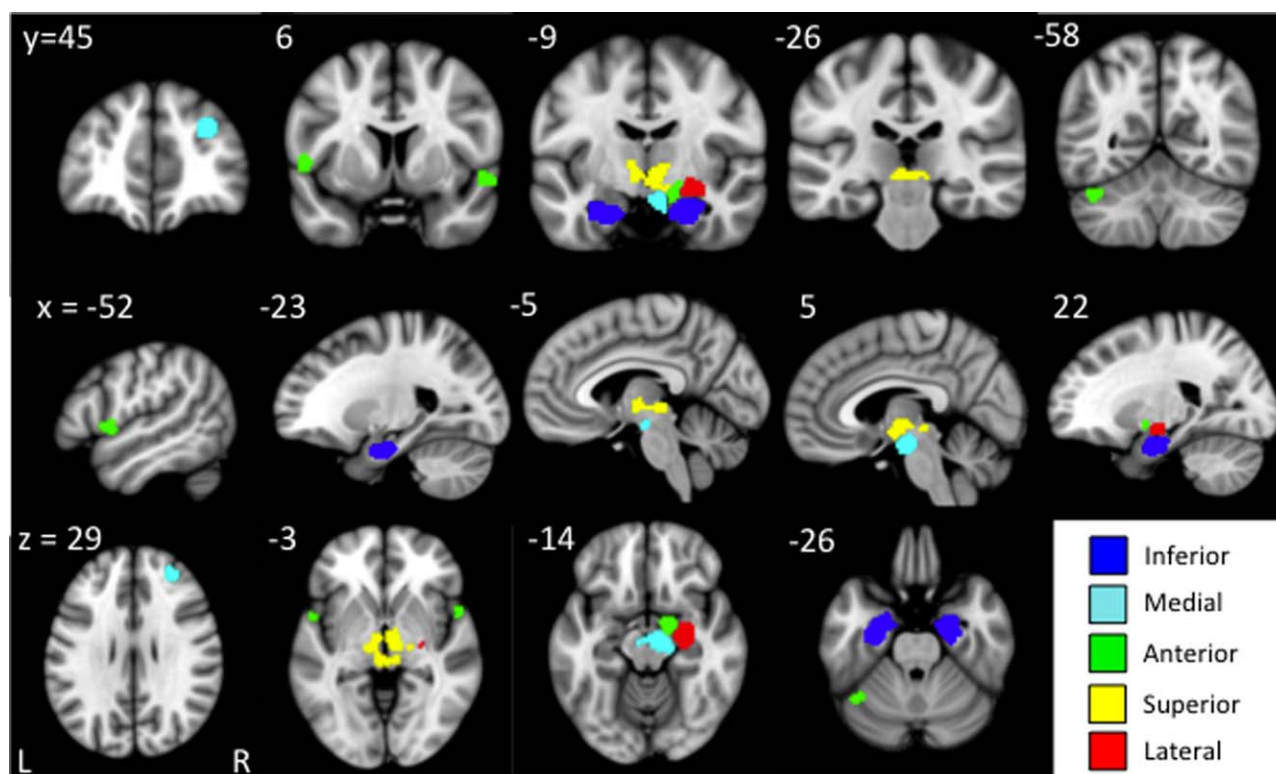
Figure 6.

Right pulvinar cluster specific task-based coactivation. For further description, cf. Results and Discussion. Slice position (given by x, y, or z location) corresponds to the Montreal Neuroimaging Institute's (MNI-152) template space.

the Morel regions (∼1,550 voxels), was divided nearly equally among the five MACM-CBP clusters. This suggests that while a smaller cytoarchitectural region is relatively functionally homogenous, a larger region represents more varied network interactions. The inclusion of multiple cytoarchitectural regions in the inferior, anterior, and lateral MACM-CBP clusters (both hemispheres) is consistent with previous reports that cytoarchitecture borders do not necessarily describe functional borders, as discussed below.

Pulvinar Cluster Correspondence with Shipp Model

Shipp [2001, 2003] summarized the non-human primate pulvinar functional anatomy in terms of several general connectivity gradients with the cortex. In particular, anterior (and lateral) parts of the pulvinar are more likely to be connected with the posterior cortex, while posterior (and medial) pulvinar are more likely to be connected with the anterior cortex. In the remaining axis, dorsal, and ventral parts of the pulvinar are more likely to connect with the dorsal and ventral cortex, respectively. These gradients did not respect the traditional cytoarchitectural sub-

divisions, but could be reconciled with chemoarchitectural subdivisions [Gutierrez et al., 1995, 2000; Shipp, 2003] that can be recognized in the human pulvinar [Cola et al., 1999]. The foci of cortical coactivation reported in our analysis do not immediately suggest the connectional gradients described by Shipp. This is perhaps a limitation of the meta-analytic process, which is intended to identify clusters of similar statistically significant coactivations (i.e., not connectivity gradients) or perhaps due to the pulvinar's phylogenic expansion [Letinic and Rakic, 2001]. Consistent with Shipp's model, we report regional pulvinar specialization that is supported by human pulvinar lesion-deficit associations [Arend et al., 2008], further described below.

Automated Behavioral Interpretation: Null Result

Meta-data analyses were used for several levels of behavioral interpretation. Behaviorally filtered MACM yielded informative results (discussed below) for separate behavioral domains. Behavioral interpretation of individual MACM-CBP clusters, however, was unsuccessful. This null result suggests each pulvinar cluster–despite

exhibiting distinct coactivation profiles–is engaged by a sufficiently wide range of behaviors to preclude unique characterization with this data-mining approach. Another interpretation is that the meta-data taxonomy utilized [Fox et al., 2005] is not sufficiently deep to capture the functional specificity of the pulvinar subregions. In either instance, an alternative strategy for behavioral interpretations was required. As an established alternative, we turn to the literature for a behavioral interpretation of the MACM-CBP clusters; this is intended not simply as speculation but as a synthesis of the literature in light of the present MACM-CBP.

Pulvinar as Exogenous Visual Attention Center

Exogenous visual attention is driven by bottom-up visual input that, once detected, reflexively guides attention allocation. MACM-CBP showed pulvinar coactivation in areas implicated in selecting and shifting visual attention [Akshoomoff and Courchesne, 1992; Berman and Wurtz, 2011]; namely, the R anterior, superior, medial, and lateral clusters coactivated with the superior colliculus, basal ganglia, and cerebellum.

Notably, the behaviorally filtered MACM reported pulvinar coactivation with occipital visual areas only in relation to the "Cognition" behavioral domain (cf. Fig. 1). This is a revealing contrast from a previous analysis of the entire BrainMap database wherein strong visual area activation with the "Perception_Vision" behavioral domain was reported [Smith et al., 2009]. In addition, individual MACM-CBP clusters surprisingly did not report coactivation with visual areas in either cluster-specific or conjunction analyses (see Figs. 4–6). Although there is abundant evidence that visual areas coactivate with the pulvinar (which we validated in an ancillary MACM of visual areas reported in Smith et al. [2009]), our results indicate that visual areas represent a small (statistically nonsignificant) portion of the pulvinar's overall coactivation profile as reported in the functional neuroimaging literature. For example, although searching BrainMap with the bilateral pulvinar seed (see Methods, Fig. 1) returns 1,991 papers reporting 66,657 coactivation locations from 7,772 experiments, seeding BrainMap with the primary visual cortex (defined by Talairaich Daemon Brodmann 17) returns only 512 papers reporting 11,792 coactivated locations from 801 experiments. The pulvinar's involvement in a subset of brain-wide cognitive processes that act independently of the visual cortex (as reported here) could explain this discrepancy. This discrepancy could also be a result of experimental contrasts wherein visual paradigms statistically "filter out" visual but not pulvinar activation.

Pulvinar as Endogenous Visual Attention Center

Endogenous visual attention is driven by top-down cognitive processes that select conscious percepts based on an individual's past experiences and immediate goals. The MACM-CBP pulvinar clusters coactivated with regions commonly involved in emotion, executive control, and memory networks.

Emotional salience heavily influences visual attention allocation. MACM showed lateralized R pulvinar coactivation with common emotional centers (R inferior cluster, bilateral amygdala; entire R pulvinar with substantia nigra) reported functional neuroimaging tasks [Ward et al., 2007].

Executive control networks provide top-down regulation to visual attention and have been divided into frontoparietal and cingulo-opercular components [Dosenbach et al., 2008; Petersen and Posner, 2012]. MACM revealed pulvinar coactivation with cingulo-opercular network areas (the L medial cluster with the anterior insula; L anterior cluster, medial superior frontal cortex; entire L pulvinar, anterior insula; entire R pulvinar, prefrontal cortex), suggesting specific pulvinar clusters could be studied within the context of the cingulo-opercular network.

Memory, both working and long-term, forms the foundation of visual recognition by imbuing percepts with meaning. Arcaro et al. [2009] recently studied the posterior parahippocampus as an object recognition center and reported variable functional anatomy along this area's superior/inferior axis. MACM showed task-based coactivation of the L lateral pulvinar cluster with the superoposterior parahippocampus and L inferior cluster with the inferoposterior parahippocampus, capturing the superior/inferior functional axis in terms of variable pulvinar connectivity.

Pulvinar in Spatial Neglect

Spatial neglect is a characteristic failure to attend and respond to environmental stimuli contralateral to a brain lesion, perhaps by interfering with healthy attention network interactions [Corbetta and Shulman, 2011]. Pulvinar-specific lesions are associated with deficits in emotion recognition [Ward et al., 2007], spatial coding, feature binding [Ward et al., 2002], and temporal coding of visual information [Arend et al., 2008]. Importantly, pulvinar lesions produce regionally dissociable deficit patterns [Arend et al., 2008], indicating subregions act independently within distinct networks. Because MACM-CBP pulvinar clusters represent distinct components of this network, they could be used as seed regions to investigate specific network components in cases of neglect.

Pulvinar as Meta-Controller of Attention

The number and organization of attention control networks remains controversial. Corbetta and Shulman [2002] have proposed attention is mediated by a dorsal and ventral network representing endogenous and exogenous processes, respectively. Posner and Petersen [1990] have

proposed attention control is mediated by anatomically separate alerting, orienting, and executive control networks. Both of these models suggest the anterior insula, anterior cingulate, lateral frontal cortex, and basal ganglia are major components of networks that control attention. Provocatively, MACM-CBP reports lateralized and cluster-specific pulvinar coactivation with each of these control network components (the entire R pulvinar with the bilateral basal ganglia; entire L pulvinar, L anterior insula; L medial pulvinar cluster, bilateral anterior cingulate) and suggests the pulvinar could be a mediator between these networks. The behaviorally filtered MACM also reported R and L pulvinar coactivation with networks involved in action, cognition, emotion, and perception, further emphasizing the pulvinar's involvement in brain-wide networks. It is well established that the pulvinar's central location allows it to economically mediate and integrate cortical-cortical activity, which mediates attention processing [Shipp, 2003]. The pulvinar synchronizes cortical activity based on attention allocation [Saalmann et al., 2012], further suggesting that the pulvinar could not only be an influential component in but a meta-controller of the attention control networks.

Methodological Considerations

This paper has presented a functional subdivision of the pulvinar based on the coactivation of experimentally induced brain activity. An implicit limitation of coactivation studies is that they do not imply monosynaptic or direct anatomical connectivity. Rather, coactivation studies may represent both direct and indirect linkages within functionally specific networks. As such, the pulvinar subdivisions and their respective coactivation networks may represent polysynaptic, indirect networks that may disobey certain "rules" for pulvinar anatomical connectivity, namely the absence of direct intrathalamic connections (e.g., the L pulvinar superior cluster coactivation network) and the absence of anatomical connections with contrahemispheric structures (e.g., many of the pulvinar clusters). That MACM-CBP did not observed connectivity gradients as described Shipp [2001, 2003] could additionally be due to the inclusion of polysynaptic connections in MACM-CBP while the Shipp [2001, 2003] connectivity gradients were based on monosynaptic tracer studies.

Connectivity-based parcellation approaches have been applied to diffusion tractography [Jbabdi et al., 2009], resting state functional connectivity [Kim et al., 2010], and MACM [Eickhoff et al., 2011] to define a region's functional anatomy. MACM coactivation profiles have been validated by multiple modalities (cf. Methods). As applied here, MACM-CBP offers specific advantages over other connectivity-based parcellation techniques. First, MACM-CBP results generalize across intergroup neuroanatomical differences and, conceivably, across genetic trends by synthesizing ∼30,000 subjects from across the globe. These results, therefore, are highly likely to be applicable to other groups and to individual patients. Second, because each MACM-CBP cluster was subsequently defined in terms of its cortical projections, the functional interactions of each pulvinar cluster can be tested in subsequent analyses. In particular, clinical investigations (e.g., in schizophrenia, epilepsy, attention deficit disorder) could assess network lesion and disease effects of each MACM-CBP cluster with its cortical projections. To this end, image volumes containing the clusters and cluster-specific coactivation pattern in standardized space will be uploaded to the BrainMap website (brainmap.org) where they can be downloaded freely and exploited.

REFERENCES

Akshoomoff NA, Courchesne E (1992): A new role for the cerebellum in cognitive operations. Behav Neurosci 106:731–738.

Arcaro MJ, McMains SA, Singer BD, Kastner S (2009): Retinotopic organization of human ventral visual cortex. J Neurosci 29: 10638–10652.

Arend I, Rafal R, Ward R (2008): Spatial and temporal deficits are regionally dissociable in patients with pulvinar lesions. Brain 131:2140–2152.

Barron DS, Tandon N, Lancaster JL, Fox PT (2014): Thalamic structural connectivity in medial temporal lobe epilepsy. Epilepsia 55:e50–e55.

Berman RA, Wurtz RH (2011): Signals conveyed in the pulvinar pathway from superior colliculus to cortical area MT. J Neurosci 31:373–384.

Byne W, Buchsbaum MS, Kemether E, Hazlett EA, Shinwari A, Mitropoulou V, Siever LJ (2001): Magnetic resonance imaging of the thalamic mediodorsal nucleus and pulvinar in schizophrenia and schizotypal personality disorder. Arch Gen Psychiatry 58:133–140.

Bzdok D, Laird AR, Zilles K, Fox PT, Eickhoff SB (2013): An investigation of the structural, connectional, and functional subspecialization in the human amygdala. Hum Brain Mapp 34:3247–3266.

Bzdok D, Langner R, Schilbach L, Jakobs O, Roski C (2013): Characterization of the temporo-parietal junction by combining data-driven parcellation, complementary connectivity analyses, and functional decoding. NeuroImage 81:381–392.

Cauda F, Cavanna AE, D'agata F, Sacco K, Duca S, Geminiani GC (2011): Functional connectivity and coactivation of the nucleus accumbens: A combined functional connectivity and structure-based meta-analysis. J Cogn Neurosci 23:2864–2877.

Chalfin BP, Cheung DT, Muniz JAPC, de Lima Silveira LC, Finlay BL (2007): Scaling of neuron number and volume of the pulvinar complex in new world primates: Comparisons with

humans, other primates, and mammals. J Comp Neurol 504: 265–274.

Cieslik EC, Zilles K, Caspers S, Roski C, Kellermann TS, Jakobs O, Langner R, Laird AR, Fox PT, Eickhoff SB (2013): Is there "One" DLPFC in cognitive action control? evidence for heterogeneity from co-activation-based parcellation. Cereb Cortex 23: 2677–2689.

Clos M, Amunts K, Laird AR, Fox PT, Eickhoff SB (2013): Tackling the multifunctional nature of Broca's region meta-analytically: Co-activation-based parcellation of area 44. NeuroImage 83:174–188.

Cola MG, Gray DN, Seltzer B, Cusick CG (1999): Human thalamus: neurochemical mapping of inferior pulvinar complex. NeuroReport 10:3733–3738.

Corbetta M, Shulman GL (2002): Control of Goal-Directed and Stimulus-Driven Attention in the Brain. Nature Reviews of Neuroscience 3:201–215.

Corbetta M, Shulman GL (2011): Spatial neglect and attention networks. Annu Rev Neurosci 34:569–599.

Dosenbach NUF, Fair DA, Cohen AL, Schlaggar BL, Petersen SE (2008): A dual-networks architecture of top-down control. Trends Cogn Sci (Regul Ed) 12:99–105.

Eickhoff SB, Laird AR, Grefkes C, Wang LE, Zilles K, Fox PT (2009): Coordinate-based activation likelihood estimation meta-analysis of neuroimaging data: A random-effects approach based on empirical estimates of spatial uncertainty. Hum Brain Mapp 30:2907–2926.

Eickhoff SB, Jbabdi S, Caspers S, Laird AR, Fox PT, Zilles K, Behrens TEJ (2010): Anatomical and functional connectivity of cytoarchitectonic areas within the human parietal operculum. J Neurosci 30:6409–6421.

Eickhoff SB, Bzdok D, Laird AR, Roski C, Caspers S, Zilles K, Fox PT (2011): Co-activation patterns distinguish cortical modules, their connectivity and functional differentiation. NeuroImage 57:938–949.

Eickhoff SB, Bzdok D, Laird AR, Kurth F, Fox PT (2012): Activation likelihood estimation meta-analysis revisited. NeuroImage 59:2349–2361.

Felleman DJ, Van Essen DC (1991): Distributed hierarchical processing in the primate cerebral cortex. Cereb Cortex 1:1–47.

Fox PT, Laird AR, Fox SP, Fox PM, Uecker AM, Crank M, Koenig SF, Lancaster JL (2005): Brainmap taxonomy of experimental design: Description and evaluation. Hum Brain Mapp 25:185–198.

Gutierrez C, Yaun A, Cusick CG (1995): Neurochemical subdivisions of the inferior pulvinar in macaque monkeys. J Comp Neurol 363:545–562.

Gutierrez C, Cola MG, Seltzer B, Cusick C (2000): Neurochemical and connectional organization of the dorsal pulvinar complex in monkeys. J Comp Neurol 419:61–86.

Ivanov I, Bansal R, Hao X, Zhu H, Kellendonk C, Miller L, Sanchez-Pena J, Miller AM, Chakravarty MM, Klahr K, Durkin K, Greenhill LL, Peterson BS (2010): Morphological abnormalities of the thalamus in youths with attention deficit hyperactivity disorder. Am J Psychiatry 167:397–408.

Jbabdi S, Woolrich M, Behrens T (2009): Multiple-subjects connectivity-based parcellation using hierarchical Dirichlet process mixture models. NeuroImage 44:373–384.

Kahnt T, Chang LJ, Park SQ, Heinzle J, Haynes J-D(2012): Connectivity-based parcellation of the human orbitofrontal cortex. J Neurosci 32:6240–6250.

Kelly C, Uddin LQ, Shehzad Z, Margulies DS, Castellanos FX, Milham MP, Petrides M (2010): Broca's region: Linking human brain functional connectivity data and non-human primate tracing anatomy studies. Eur J Neurosci 32:383–398.

Kim J-H, Lee J-M, Jo HJ, Kim SH, Lee JH, Kim ST, Seo SW, Cox RW, Na DL, Kim SI, Saad ZS (2010): Defining functional SMA and pre-SMA subregions in human MFC using resting state fMRI: Functional connectivity-based parcellation method. NeuroImage 49:2375–2386.

Koski L, Paus T (2000): Functional connectivity of the anterior cingulate cortex within the human frontal lobe: A brain-mapping meta-analysis. Exp Brain Res 133:55–65.

Krauth A, Blanc R, Poveda A, Jeanmonod D, Morel A, Székely G (2010): A mean three-dimensional atlas of the human thalamus: Generation from multiple histological data. NeuroImage 49:2053–2062.

Laird AR, Eickhoff SB, Fox PM, Uecker AM, Ray KL, Saenz JJ, McKay DR, Bzdok D, Laird RW, Robinson JL, Turner JA, Turkeltaub PE, Lancaster JL, Fox PT (2011): The BrainMap strategy for standardization, sharing, and meta-analysis of neuroimaging data. BMC Res Notes 4:349.

Lancaster JL, Laird AR, Eickhoff SB, Martinez MJ, Fox PM, Fox PT (2012): Automated regional behavioral analysis for human brain images. Front Neuroinform 6:1–12.

Leh SE, Chakravarty MM, Ptito A (2008): The connectivity of the human pulvinar: A diffusion tensor imaging tractography study. Int J Biomed Imag 2008:1–5.

Letinic K, Rakic P (2001): Telencephalic origin of human thalamic GABAergic neurons. Nat Neurosci 4:931–936.

Mitelman SA, Byne W, Kemether EM, Hazlett EA, Buchsbaum MS (2006): Correlations between volumes of the pulvinar, centromedian, and mediodorsal nuclei and cortical Brodmann's areas in schizophrenia. Neurosci Lett 392:16–21.

Morel A, Magnin M, Jeanmonod D (1997): Multiarchitectonic and stereotactic atlas of the human thalamus. J Comp Neurol 387: 588–630.

Narayana S, Laird AR, Tandon N, Franklin C, Lancaster JL, Fox PT (2012): Electrophysiological and functional connectivity of the human supplementary motor area. NeuroImage 62:250–265.

Olszewski J (1952): The Thalamus of the Macaca, Mulatta: An Atlas for Use With the Stereotaxic Instrument. Basel: Karger Publishers.

Paus T, Jech R, Thompson CJ, Comeau R, Peters T, Evans AC (1997): Transcranial magnetic stimulation during positron emission tomography: A new method for studying connectivity of the human cerebral cortex. J Neurosci 17:3178–3184.

Petersen SE, Posner MI (2012): The attention system of the human brain: 20 years after. Annu Rev Neurosci 35:73–89.

Posner MI, Dehaene S (1994): Attentional networks. Trends Neurosci 17:75–79.

Posner MI, Petersen SE (1990): The Attention System of the Human Brain. Annual Reviews of Neuroscience 13:25–42.

Robinson DL, Petersen SE (1992): The pulvinar and visual salience. Trends Neurosci 15:127–132.

Robinson JL, Laird AR, Glahn DC, Lovallo WR, Fox PT (2010): Metaanalytic connectivity modeling: Delineating the functional connectivity of the human amygdala. Hum Brain Mapp 31: 173–184.

Robinson JL, Laird AR, Glahn DC, Blangero J, Sanghera MK, Pessoa L, Fox PM, Uecker A, Friehs G, Young KA, Griffin JL, Lovallo WR, Fox PT (2012): The functional connectivity of the

human caudate: An application of meta-analytic connectivity modeling with behavioral filtering. NeuroImage 60:117–129.

Romanski LM, Giguere M, Bates JF, Goldman-Rakic PS (1997): Topographic organization of medial pulvinar connections with the prefrontal cortex in the rhesus monkey. J Comp Neurol 379:313–332.

Rosenberg DS, Mauguiere F, Catenoix H, Faillenot I, Magnin M (2009): Reciprocal thalamocortical connectivity of the medial pulvinar: A depth stimulation and evoked potential study in human brain. Cereb Cortex 19:1462–1473.

Rotshtein P, Soto D, Grecucci A, Geng JJ, Humphreys GW (2011): The role of the pulvinar in resolving competition between memory and visual selection: A functional connectivity study. Neuropsychologia 49:1544–1552.

Rottschy C, Caspers S, Roski C, Reetz K, Dogan I, Schulz JB, Zilles K, Laird AR, Fox PT, Eickhoff SB (2013): Differentiated parietal connectivity of frontal regions for "what" and 'where' memory. Brain Struct Funct 218:1551–1567.

Saalmann YB, Kastner S (2011): Cognitive and perceptual functions of the visual thalamus. Neuron 71:209–223.

Saalmann YB, Pinsk MA, Wang L, Li X, Kastner S (2012): The pulvinar regulates information transmission between cortical areas based on attention demands. Science 337:753–756.

Shipp S (2003): The functional logic of cortico-pulvinar connections. Philos Trans R Soc Biol Sci 358:1605–1624.

Shipp S (2004): The brain circuitry of attention. Trends Cogn Sci (Regul Ed) 8:223–230.

Smith SM, Fox PT, Miller KL, Glahn DC, Fox PM, Mackay CE, Filippini N, Watkins KE, Toro R, Laird AR (2009): Correspondence of the brain's functional architecture during activation and rest. Proc Natl Acad Sci 106:13040–13045.

Stein T, Moritz C, Quigley M, Cordes D, Haughton V, Meyerand E (2000): Functional connectivity in the thalamus and hippocampus studied with functional MR imaging. AJNR Am J Neuroradiol 21:1397–1401.

Toro R, Fox PT, Paus T (2008): Functional coactivation map of the human brain. Cerebral Cortex 18:2553–2559.

Turkeltaub PE, Eden GF, Jones KM, Zeffiro TA (2002): Meta-analysis of the functional neuroanatomy of single-word reading: Method and validation. NeuroImage 16:765–780.

Turkeltaub PE, Eickhoff SB, Laird AR, Fox M, Wiener M, Fox P (2012): Minimizing within-experiment and within-group effects in activation likelihood estimation meta-analyses. Hum Brain Mapp 33:1–13.

Ward R, Danziger S, Owen V, Rafal R (2002): Deficits in spatial coding and feature binding following damage to spatiotopic maps in the human pulvinar. Nat Neurosci 5:99–100.

Ward R, Calder AJ, Parker M, Arend I (2007): Emotion recognition following human pulvinar damage. Neuropsychologia 45: 1973–1978.

Wilke M, Turchi J, Smith K, Mishkin M, Leopold DA (2010): Pulvinar inactivation disrupts selection of movement plans. J Neurosci 30:8650–8659.